Scripta Materialia 110 (2016) 28–32

Contents lists available at ScienceDirect

Scripta Materialia

journal homepage: www.elsevier.com/locate/scriptamat

Structure and dynamics of shear bands in amorphous–crystalline nanolaminates

Wei Guo [a,c,*], Bin Gan [b], Jon M. Molina-Aldareguia [b], Jonathan D. Poplawsky [c], Dierk Raabe [a]

[a] Department of Microstructure Physics and Alloy Design, Max-Planck Institut für Eisenforschung, Düsseldorf 40237, Germany
[b] IMDEA Materials Institute, C/Eric Kandel 2, Getafe, Madrid 28906, Spain
[c] Center for Nanophase Materials Sciences, Oak Ridge National Laboratory, Oak Ridge, 37831 TN, USA

ARTICLE INFO

Article history:
Received 6 July 2015
Revised 22 July 2015
Accepted 28 July 2015
Available online 3 August 2015

Keywords:
Nanolaminates
Metallic glass
Nanocrystallization
Shear band
Atom probe tomography

ABSTRACT

The velocities of shear bands in amorphous CuZr/crystalline Cu nanolaminates were quantified as a function of strain rate and crystalline volume fraction. A rate-dependent transition in flow response was found in a 100 nm CuZr/10 nm Cu nanolaminates. When increasing the Cu layer thickness from 10 nm to 100 nm, the instantaneous velocity of the shear band in these nanolaminates decreases from 11.2 μm/s to <~500 nm/s. Atom probe tomography and transmission election microcopy observation revealed that in post-deformed pillars both grain rotation in the crystalline portion and non-diffusive crystallization in the amorphous layer affect the viscosity of shear bands.

At room temperature, the plasticity of metallic glasses (MGs) is mainly achieved by the initiation and propagation of nanometer sized shear bands [1]. Establishing a fundamental understanding of these shear bands and controlling them for avoiding catastrophic propagation are particularly urgent before rendering MGs into the class of advanced structural/functional materials. Therefore, multiple studies have addressed the structural [2], chemical [3] and dynamic properties [4] of shear bands. Shear bands are also considered to be possible sites for nanocrystallization in systems such as Al-based [5] and Zr-based metallic glasses [6]. The strain induced devitrification process has been observed in nanoindentation [7], uniaxial compression [8] and cold rolling [9] of metallic glasses. However, it is still unclear whether nucleation of crystalline phases is driven by adiabatic heating [10] or by the increase of free volume [11]. The role of these crystalline phases in influencing the shear band propagation is also unknown owing to the lack of structural and chemical information about shear bands.

At least the introduction of known crystalline phases into an amorphous matrix promises an enhanced plasticity [12] by forming multiple shear bands or a dislocation/shear mediated co-deformation process [13]. The morphology of the shear bands is highly dependent on the crystalline phase fraction, by which the shear band dynamics is highly influenced. Some pioneering studies on pure metallic glasses reveal that a single shear band can propagate 0.3–14 μm within a millisecond [14,15], but little work was done for the metallic glass/crystalline nanocomposite structures.

In this study, a quantitative assessment of the shear band dynamics in 100 nm amorphous CuZr/x nm crystalline Cu (x = 10, 50, 100 nm) nanolaminates within a time interval of 10^{-2} ms was carried out. Transmission Electron Microscopy (TEM) and Atom Probe Tomography (APT) were jointly used for evaluating additional structural and chemical features of shear bands after deformation.

Amorphous CuZr/crystalline Cu nanolaminates were deposited on Si (100) wafers by direct current magnetron sputtering. For these nanolaminates, the thickness of the individual amorphous CuZr layers were fixed to 100 nm, while the thickness of the nanocrystalline Cu layers varied between 10, 50 and 100 nm. Accordingly, the samples are referred to as MS10, MS50 and MS100, respectively. The materials synthesis and the micropillar preparation with a focused Ion Beam (FIB) are described in Ref. [13]. The micropillars were compressed using a circular flat punch of 10 μm in diameter inside an instrumented nanoindentation system (Hysitron TI950) in load control mode. The tests were interrupted at specific load levels. The imposed strain rate varied from 6×10^{-4} s^{-1} to 6×10^{-2} s^{-1} with a data

* Corresponding author at: Department of Microstructure Physics and Alloy Design, Max-Planck Institut für Eisenforschung, Düsseldorf 40237, Germany.
E-mail address: wguo2007@gmail.com (W. Guo).

http://dx.doi.org/10.1016/j.scriptamat.2015.07.038
1359-6462/

sampling rate of 30 kHz. The morphology of the micropillars prior to and after the deformation was observed with a FEI Helios Nanolab 600i instrument.

The engineering stress, $\sigma = F/A_0$, was calculated from the measured force F and the pillar cross-sectional area A_0 at 20% of its height away from the top of the pillar, since the tapered geometry confines deformation to the top. For calculating the engineering strain, the displacement was firstly corrected by [16,17]:

$$L = L_{\text{meas}} - \frac{(1-\nu_i^2)P}{E_i d_i} - \frac{(1-\nu_{si}^2)P}{E_{si} d_{si}} \quad (1)$$

where P is the applied load, d_i and d_{si} are the diameter of the pillar at the top and bottom, respectively. E_i and E_{si} are the Young's modulus of diamond (1440 GPa [18]) and of the (100) Si substrate (130 GPa [19]), respectively. $\nu_i \approx 0.2$ and $\nu_{Si} = 0.278$ [20] are the Poisson's ratio of diamond and of the Si substrate, respectively. The engineering strain is obtained by dividing the corrected displacement by the film thickness.

TEM lamellae and APT tips containing the deformed pillars were prepared site-specific by an *in situ* lift-out method and FIB milling [21,22]. A 200 kV Jeol JEM-2200FS TEM was used for high-resolution TEM imaging. APT was performed with a local electrode atom probe (CAMECA LEAP 3000X HR). Samples were analyzed at a base temperature of 60 K, applying 532 nm wavelength 10 ps laser pulses of 0.4 nJ with at a repetition rate of 250 kHz. The datasets were reconstructed and analyzed using the IVAS 3.6.8 software (CAMECA Instruments).

Fig. 1(a–c) shows the morphologies of post-deformed pillars for three sample types. The shapes of pillars deformed at different strain rates are similar. Hence only one representative image of the deformed micropillars is shown for each system. As shown by these SEM micrographs, the MS10 pillars experience only one major shear band which leads to large displacement bursts. In contrast, the compressed MS50 and MS100 pillars show multiple confined shear bands, nucleated from the topmost amorphous layer. These differences are consistent with the engineering stress–strain profiles, i.e. the stress–strain curves of these two material systems have a smooth shape.

A threshold measure of 5% plastic strain was selected as reference point to compare the flow stress ($\sigma_{0.05}$) and strain rate sensitivity (m) values for the different systems. As shown in Fig. 1d, at 5% strain, the flow stresses in the MS10 pillars decreases when the strain rate ($\dot{\varepsilon}$) is increased from $6 \times 10^{-4}\,s^{-1}$ to $6 \times 10^{-2}\,s^{-1}$. As rationalized by $m = \frac{\partial \ln \sigma_{0.05}}{\partial \ln \dot{\varepsilon}}$, the MS10 pillars have a strain rate sensitivity of −0.003. In contrast, the MS50 and MS100 samples have m values between 0.009 and 0.016, which fit into the range of m values found for pure nanocrystalline/ultrafine grain materials at ambient temperature [23]. This observation indicates that the crystalline mediated plasticity initially dominates the plastic flow for MS50 and MS100 nanocomposites.

Note that although the stress strain curve may look rather smooth, the local flow events are not smooth at all [24–26]. The fast control loop of the TI 950 nanoindentation system with a data acquisition rate of 30 kHz enables us to quantify the instantaneous velocity of shear band propagation. Knowing from Fig. 1a that the initial plastic strain of the MS10 pillar is mainly carried by one single shear band, we can calculate its velocity as, $v_{SB} = \sqrt{2} \times \Delta u/\Delta t$ where $\sqrt{2}$ is a geometrical factor assuming a 45° angle between shear-plane and loading axis, Δu is the displacement jump, and Δt is the time elapsed during this event. For the MS10 pillars no single shear band displacement burst is observed when deformed at a strain rate of $6 \times 10^{-4}\,s^{-1}$ (Fig. 2a). However, as evident from Fig. 2b and c, the increase of the strain rate from 6×10^{-3} to 6×10^{-2} can accelerate the instantaneous velocity of shear band from ~100 nm/s to 11 μm/s for the MS10 sample, which is only one or two orders of magnitude lower than that for pure metallic glasses [4,14]. Although multiplication of shear bands can be observed when deforming the MS50 and MS100 samples, a displacement burst corresponding to a single shear band propagation was not observed. This indicates that sufficiently thick crystalline layers can slow down the instantaneous velocity of shear band propagation to a range close to externally applied cross-head velocities.

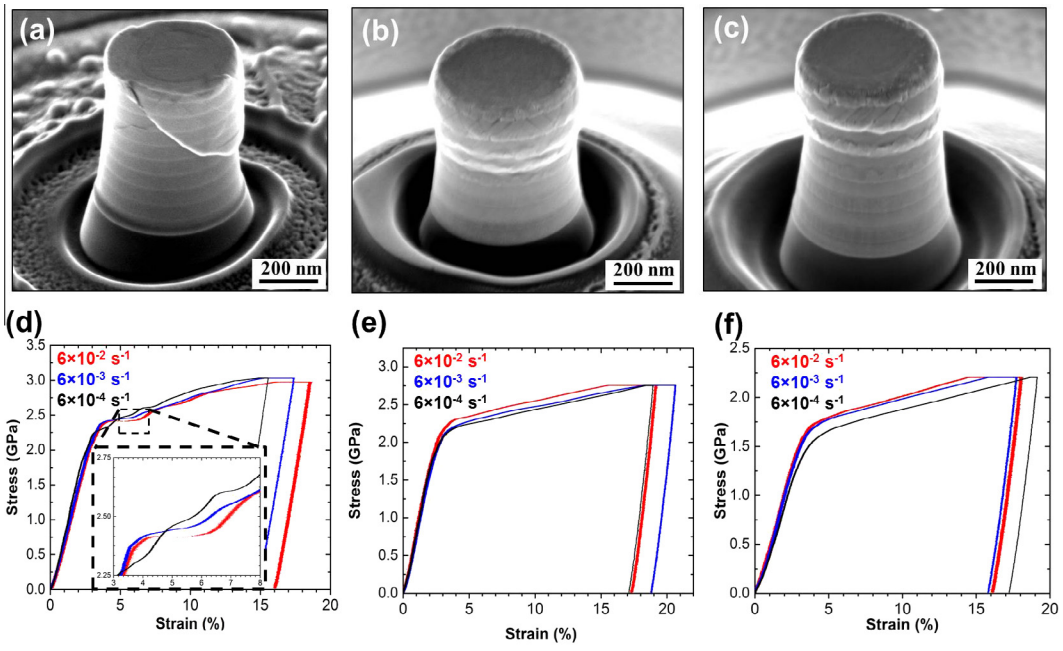

Fig. 1. (a–c) SEM images of ~600 nm diameter pillars after ~15% compression. (a) 100 nm amorphous CuZr/10 nm Cu (MS10). (b) 100 nm amorphous CuZr/50 nm Cu(MS50). (c) 100 nm amorphous CuZr/100 nm Cu(MS100). Also shown are the stress–strain curves of (d) MS 10, (e) MS50, and (f) MS 100 pillars compressed to 15–20% strain with different strain rates.